Neuroscience Letters 746 (2021) 135665

Contents lists available at ScienceDirect

Neuroscience Letters

journal homepage: www.elsevier.com/locate/neulet

Blood-brain barrier permeability towards small and large tracers in a mouse model of osmotic demyelination syndrome

Joshua Scalisi [a,b], Benoît Balau [a], Lynn Deneyer [a,b], Joanna Bouchat [a], Jacques Gilloteaux [a,c], Charles Nicaise [a,*]

[a] URPhyM – NARILIS, Université de Namur, Namur, Belgium
[b] HEPH-Condorcet, Catégorie Paramédicale Charleroi, Charleroi, Belgium
[c] Department of Anatomical Sciences, St George's University School of Medicine, Newcastle upon Tyne, United Kingdom

ARTICLE INFO

Keywords:
Blood-brain barrier
Tracer
Permeability
Endothelium
Osmotic demyelination syndrome
Mouse

ABSTRACT

During osmotic demyelination syndrome (ODS), myelin and oligodendrocyte are lost according to specific patterns in centro- or extra-pontine regions. In both experimental model of ODS and human cases, brain lesions are locally correlated with the disruption of the blood brain-barrier (BBB). The initiation, the degree and the duration of blood-brain barrier (BBB) opening as well as its contribution to brain damages are still a matter of debate. Using a panel of intravascular tracers from low- to high- molecular weight (from 0.45 kDa 150 kDa), we have assessed the BBB permeability at different timings of ODS induced experimentally in mice. ODS was mimicked according to a protocol of rapid correction of a chronic hyponatremia. We demonstrated that BBB leakage towards smallest tracers Lucifer Yellow (0.45 kDa) and Texas Red-dextran (3 kDa) was delayed by 36 h compared to the first clues of oligodendrocyte loss (occurring 12 h post-correction of hyponatremia). At 48 h post-correction and concomitantly to myelin loss, BBB was massively disrupted as attested by accumulation of Evans Blue (69 kDa) and IgG (150 kDa) in brain parenchyma. Analysis of BBB ultrastructure verified that brain endothelial cells had minimal alterations during chronic hyponatremia and at 12 h post-correction of hyponatremia. However, brain endothelium yielded worsened alterations at 48 h, such as enlarged vesicular to tubular-like cytoplasmic profiles of pinocytosis and/or transcytosis, local basal laminae abnormalities and sub-endothelial cavities. The protein expressions of occludin and claudin-1, involved in inter-endothelial tight junctions, were also downregulated at 48 h post-correction of hyponatremia. Our results revealed that functional BBB opening occured late in pre-established ODS lesions, and therefore was not a primary event initiating oligodendrocyte damages in the mouse model of ODS.

1. Introduction

Osmotic demyelination syndrome (ODS) is a brain demyelinating disease that usually occurs as a result of an abrupt correction of a chronic hyponatremia [1,2]. Besides myelin and oligodendrocytes are the major targets of the disorder, recent reports from human cases and experimental models converge to say that astrocytes are concomitantly damaged or lost inside the demyelinating lesions [3–7]. One of the most intriguing feature is the peculiar pattern of demyelination throughout susceptible regions of the CNS. Related to their neurologic symptoms, patients display demyelinating lesions in either centropontine or extrapontine regions (*e.g.* basal ganglia, caudate nucleus, putamen, thalamus, internal and external capsules), or even both [8,9]. Interestingly, some brain areas are fully spared despite their high content of myelin and interfascicular oligodendrocytes.

Neuroscientists have debated about a significant contribution of blood-brain barrier (BBB) opening to myelin or oligodendrocyte damages during ODS [10–15]. Indeed, it has been well described that oligodendrocytes are vulnerable towards various non-physiological insults, such as oxidative stress, glutamate excitotoxicity, ATP release toxicity, inflammatory mediators, antibodies or complement-mediated attack, or other blood components (review in [16]). For instance, exposure to

Abbreviations: BBB, blood-brain barrier; CNS, central nervous system; L.Y., Lucifer Yellow; ODS, osmotic demyelination syndrome; T.R., Texas Red-dextran.

* Corresponding author at: Université de Namur, URPhyM – NARILIS, Rue de Bruxelles 61, B-5000, Namur, Belgium.
E-mail addresses: jo-scalisi@hotmail.com (J. Scalisi), benoit.balau@unamur.be (B. Balau), ldeneyer4@gmail.com (L. Deneyer), joanna.bouchat@unamur.be (J. Bouchat), jacques.gilloteaux@unamur.be (J. Gilloteaux), charles.nicaise@unamur.be (C. Nicaise).

https://doi.org/10.1016/j.neulet.2021.135665
Received 14 August 2020; Received in revised form 17 December 2020; Accepted 13 January 2021
Available online 23 January 2021
0304-3940/© 2021 Elsevier B.V. All rights reserved.

whole-serum or extracellular hemoglobin induces from cellular stress to death of cultured rat oligodendrocytes [17,18]. Therefore, it would make sense that blood-brain barrier (BBB) integrity be a pre-requisite for proper oligodendrocyte functioning. Interestingly, in both ODS-affected humans and animals, there is a strong correlation between the brain areas undergoing demyelination and BBB opening [10,11,19,20]. BBB permeability has been investigated in experimental models using intravascular tracers that had exuded into brain parenchyma [12–14,19,20]. So far, evidences showed that BBB leakage is delayed compared to myelin and oligodendrocyte defects. Although this suggests that BBB breach is not a primary event initiating oligodendrocyte damages, the limitation has been the usage of extravasation tracers equal or larger than 34 kDa: complement fragment C3d (34 kDa), horseradish peroxidase (44 kDa), albumin-bound Evans Blue (69 kDa), immunoglobulins G (150 kDa). Hence, it does not exclude that subtle changes in BBB permeability to molecules <34 kDa could occur very early during chronic hyponatremia or immediately after its rapid correction. If this is the case, an unidentified blood-borne toxic factor would selectively damage oligodendrocytes, precipitating their death, followed by myelinolysis. To address this question, we investigated the BBB permeability towards small- and large-molecular weight tracers at different timings after the correction of hyponatremia using the mouse model of ODS [20–22]. We also looked at the ultrastructure of brain endothelium and at the expression level of inter-endothelial tight junctions.

2. Material and methods

2.1. Animals

The experimental protocol was conducted in compliance with the European Communities Council Directives for Animal Experiment (2010/ 63/EU, 86/609/EEC and 87–848/EEC) and was approved by the Animal Ethics Committee of University of Namur (ethic project UN 14–210). Male C57BL/6 J mice, aged from 3 to 4 months were included in the study. They were housed in a temperature and humidity-controlled room maintained at 12:12 h light/dark cycle. Measures (daily monitoring, acute administration of buprenorphine: 0.1 mg/kg in case of signs of pain) and human endpoints were set to minimize pain and discomfort.

2.2. Model of ODS

ODS was induced in mice as described previously (Bouchat et al., 2018). Briefly, an osmotic minipump (Model 1004, Alzet, Cupertino, CA, USA) filled with desmopressin acetate (0.002 mg/mL) (Minirin®, Ferring, Saint-Prex, Switzerland) was inserted subcutaneously at day 0. Standard pellets and water were replaced by a low-sodium liquid diet (AIN76A, MP Biomedicals, Santa Ana, CA, USA), for a period of 4 days *ad libitum*. On the 4th day, blood serum level was measured using Spotchem EL SE-1520 electrolyte analyzer (Arkray, Kyoto, Japan) and hyponatremia, as found below 124 mEq/L, was corrected using an intraperitoneal injection of hypertonic saline (NaCl 1 M; 1.5 mL/100 g body weight). Animals were divided into four groups: normonatremic mice (NN), uncorrected 4-days hyponatremic mice (HN), ODS mice sacrificed 12 h post-correction (12 h PCHN) or 48 h post-correction (48 h PCHN). Average natremia (mean ± SEM) were respectively 146.6 ± 2.1 mEq/L for normonatremic group and 118.2 ± 1.6 mEq/L for hyponatremic group. At 12 h or 24 h after the correction of hyponatremia, natremia retrieved 146 ± 5.1mEq/L, with a mean ΔSNa + of 34.2 ± 3.3mEq/L.

2.3. Blood-brain barrier tracer procedures

Intravascular tracers were chosen according to their molecular weight gradation: Lucifer Yellow (L.Y.; 0.45 kDa, Sigma-Aldrich), Texas Red-dextran (T.R.; 3 kDa, Thermofisher Scientific #D3328), and Evans Blue (albumin-bound 68 kDa, Sigma-Aldrich).

Evans blue diluted saline solution (2% w/v) was intraperitoneally delivered (4 mL/kg) 1 h before euthanasia [23]. Euthanasia was achieved under anesthesia using ketamine (100 mg/kg) and xylazine (5 mg/kg). Mice were exsanguinated and transcardially perfused with heparinized NaCl 0.9 %, until no more blue dye flew out of the right atrium. Prosencephalons were isolated, weighted before snap-freezing into liquid nitrogen, and then stored at −80 °C until analysis. Samples were thawed, digested in 250 mL formamide for 3 days at 65 °C. Next, samples were centrifuged at 13,000 rpm for 10 min at 4 °C and supernatants analyzed with spectrophotometry at 620 nm. Dye concentration in the sample was interpolated from a standard curve and normalized with the wet weight of the tissue.

Texas Red-dextran and Lucifer Yellow were diluted in saline to respectively reach a concentration of 1 mM and 10 mM. Under anesthesia (ketamine 100 mg/kg and xylazine 5 mg/kg), a mixture (1:2) of Texas Red-dextran and Lucifer Yellow was intracardially injected (100 µL/mouse) and allowed to circulate for 15 min before euthanasia. Euthanasia was achieved by exsanguination, followed by transcardial perfusion for 1 min with heparinized NaCl 0.9 %. Prosencephalons were homogenized in PBS at 4 °C. After spinning down the samples at 10,000×*g* for 15 min at 4 °C, the supernatant was measured to obtain raw fluorescence units (RFU) in a fluorescence plate reader at excitation/emission wavelength of 425/525 nm for Lucifer Yellow and 595/625 nm for Texas Red-dextran and further normalized to the wet weight of the tissue.

2.4. Immunohistochemistry

Under anesthesia (ketamine (100 mg/kg) and xylazine (5 mg/kg)), mice were exsanguinated and transcardially perfused with NaCl 0.9 % followed by phosphate-buffered 4% paraformaldehyde. Brains were harvested and post-fixed overnight in fixative. Hemi-brains were then immunolabeled according to standard procedures and as previously described [20]. Except for IgG immunolabeling, primary antibodies were incubated overnight at 4 °C. Primary antibodies were as follow: p25alpha as marker of mature oligodendrocyte (1:1000, Sigma-Aldrich, HPA036576); PLP as marker of myelin protein (1:1000, Biorad, MCA839 G), TMEM119 as marker of microglia (1:1000, Abcam, ab209064) and Slc4a1/Band 3 as marker of erythrocyte (1:1000, Cell Signaling, #20112). Binding of primary antibody was detected using a secondary biotinylated goat anti-mouse or anti-rabbit IgG (1:100, Vectastain, Vector Laboratories, Burlingame, CA) for 1 h at room temperature. Immunoreactivity was then revealed as described elsewhere [24]. The morphology of TMEM119 microglial cells was analyzed according to Bouchat et al. [20]. For each experimental group, one hundred TMEM119^{+} cells were chosen randomly and blindly, and sorted into four types based on their morphology: Type A resting: cells have long and very thin processes; Type B ramified: processes are long and thicker, cytoplasm around nucleus is visible; Type C ramified: processes are shorter and there are many branches; Type D amoeboid: rounded hypertrophic cell without processes.

Extravasation of endogenous IgG was evidenced by immunolabeling using a biotinylated goat anti-mouse IgG (1:50; Jackson ImmunoResearch, Newmarket, UK) for 4 h at room temperature, then revealed with avidin–biotin–peroxidase (Vector Labs, Belgium) and diaminobenzidine (Dako, Belgium) including hematoxylin counterstaining. Brain tissue was imaged with an Olympus BX63 microscope using the Cell Sens software.

2.5. Western blot

Proteins were extracted from micro-dissected thalamus and resolved as previously described [20]. Primary antibodies used were rabbit anti-occludin antibody (# 40–4700, ThermoFisher, 1:500), rabbit anti-claudin-1 antibody (#71-7800, ThermoFisher, 1:1000), rabbit

anti-GLUT-1 antibody (#ab115730, Abcam, 1:1000) and mouse anti--β-actin antibody (Sigma-Aldrich A5441, 1:10 000).

2.6. Ultrastructural morphometry

Under anesthesia, mice were transcardially perfused with a solution of PFA 2% and glutaraldehyde 2% in 0.1 M phosphate buffer (pH 7.2–7.4). Thalamus, a region prone to demyelination and BBB breakdown in the mouse model of ODS was sampled according to Paxinos and Franklin's mouse brain atlas and method previously described [20–22].

All measurements were performed using manual delimitation of capillary (sub)structures, from TEM images, according to previously published procedures [25,26]. Each endothelium thickness was calculated as an average of 5 measurements in the thinnest parts associated with the marginal fold and 5 measurements in the thickest parts associated with the intercellular junctions. The basal laminae thickness was similarly measured for the sake of completion of the endothelial lining's investigations. For vesicles' density and size, the peri-nuclear organelles and adjacent perikaryon were not considered for measurements, according to other studies [25–27]. Pinocytosis and transcytosis profile structures viewed were generically named 'vesicles'. Vesicle profile surfaces were measured and averaged per μm^2 of endothelial cytoplasm, where their relative density within the same surface's section was averaged in each experimental condition.

2.7. Statistical analysis

All results were expressed as mean values ± Standard Error of Mean (SEM). The data were statistically analyzed using ANOVA followed by Dunn's multiple comparisons test. The level of significance was set at $p < 0.05$. The statistical analyses were performed by using the software GraphPad Prism version 7 (GraphPad Software, Inc., La Jolla, CA, USA).

3. Results

The mouse model of ODS was validated by assessing the extent and timing of oligodendrocyte loss and myelinolysis. Accordingly, in the thalamus - a demyelination-prone region previously reported in the mouse model - a drastic loss of proteolipid protein (PLP) immunoreactivity was observed 48 h post-correction of hyponatremia (Suppl. Fig. 1a). Unlike PLP expression, the decrease of p25alpha + oligodendrocytes occurred as early as 12 h post-correction, with no more immunoreactive cells at the 48 h timing (Suppl. Fig. 1b). Image-based quantification confirmed that myelin loss was shifted by at least 36 h

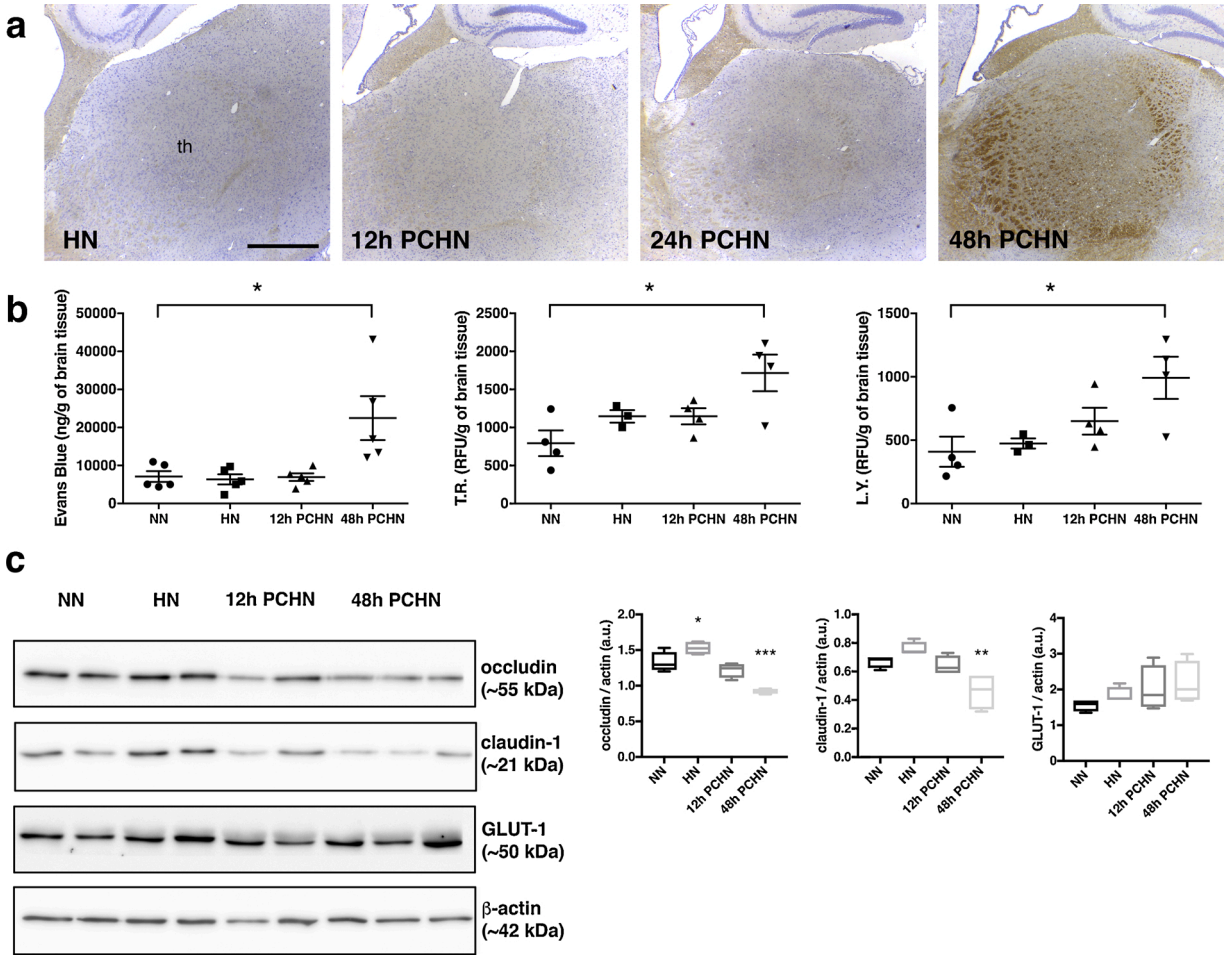

Fig. 1. BBB permeability towards various intravascular tracers in ODS brains. (a) The tracers were sorted from the highest- to the lowest molecular weight: IgG (150 kDa), Evans Blue (69 kDa), Texas Red-dextran (T.R., 3 kDa) and Lucifer Yellow (L.Y., 0.45 kDa). IgG deposits were massively detected in the thalamus (th) at 48 h PCHN. Scale bar =500 μm. (b) Significant Evans Blue extravasation was measured at 48 h PCHN in whole-brain homogenates from ODS mice compared with normonatremic mice (NN). Similarly, accumulation of T.R. or L.Y. into brain parenchyma was higher at 48 h PCHN (B). *p < .05 compared to HN group, ANOVA followed by Dunn's multiple comparisons. (c) Expression of inter-endothelial junction proteins. Protein expression of *occludin* and *claudin-1* was decreased at 48 h PCHN. No significant change was observed in GLUT-1 expression. **p < .01, ***p < .001 compared to NN group, ANOVA followed by Dunn's multiple comparisons, n = 4 independent samples per experimental condition. Results are expressed as mean +/- SEM. RFU means "relative fluorescence units" and "a.u." means "arbitrary unit".

compared to oligodendrocyte loss (Suppl. Fig. 1c). In parallel, the microglia activation was quantified in the ODS lesions. Resident TMEM119-expressing microglia started to switch toward a type B morphology within the first 12 h after the correction, with few type D cells (Suppl. Fig. 1d). It is only at a timing of 48 h that a majority of type C and type D cells were observed. At 48 h post-correction of hyponatremia, BBB breakdown was evidenced by brain parenchymal endogenous IgG deposits that were detected using an immunohistochemical method. While no IgG immunoreactivity was observed in NN, HN and 12 h post-correction, a strong immunolabeling was seen in the thalamus at 48 h post-correction of hyponatremia, that appeared more intense at the perilesional rim (Fig. 1a). Of note, immunoreactivity against slc4a1, a surface marker of erythrocytes, was not evidenced in any of the ODS samples; this certainly advocated that extravasation of erythrocytes did not occur into brain parenchyma (data not shown). Next, we sought to know whether a BBB leakage to smaller molecules than IgG (150 kDa) could have occurred earlier during the ODS induction. Evans Blue, Texas Red-dextran or Lucifer Yellow were intravascularly delivered into the different experimental groups and allowed to circulate for several minutes. Evans Blue binds to circulating albumin to form a higher molecular weight protein tracer (69 kDa), whereas Texas Red-dextran (3 kDa) or Lucifer Yellow (0.45 kDa) remain unbound small molecules. Regardless of their molecular weight and albumin binding properties, the profile of extravasation was similar for all three intravascular tracers. A significant accumulation into brain parenchyma was measured only at the timing 48 h post-correction of hyponatremia (one-way ANOVA, $p < 0.05$ 48 h PCHN compared to NN) (Fig. 1b). We next investigated how ODS induction impacted on the molecular integrity of brain endothelium, specifically in the thalamus. Remarkably, the gene expression of GLUT-1, endothelial glucose transporter expressed at luminal surface, was unchanged across the different experimental groups. On the contrary, the protein expression of claudin-1 and occludin was significantly downregulated at 48 h post-correction of hyponatremia, suggesting that, during the ODS induction, endothelial tight junctions may have been transiently destabilized (Fig. 1c).

An ultrastructural analysis of endothelium integrity and sub-endothelial components was performed on all experimental groups. Normal thalamus capillaries showed typical brain vascular linings with endothelial cells dotted with a tiny Golgi apparatus and small round to oval plasmalemmal vesicular profiles that encompassed pinocytosis and transcytosis (collectively called vesicles), as well as delineated by marginal fold extensions at the level of the inter-endothelial junctional complexes (Fig. 2 a–b). During chronic hyponatremia challenge, quasi all capillaries showed collapsed lumen where surface linings appeared squeezed together and discrete sub-endothelium voids appeared (Fig. 2 c–d). At 12 h PCHN, endothelial cells displayed numerous cytoplasm vesicles and some oblong, lysosome-like electron-dense bodies disseminated among these surface linings (Fig. 2 e–f). It is also at this stage that junctional complexes became poorly detectable as they got entwined by small troughs or vesicles. At 48 -hs post-correction of hyponatremia, endothelium vesicles increased their size, not only in the main cytoplasm and impinged as grooved parts at the level of the junctional

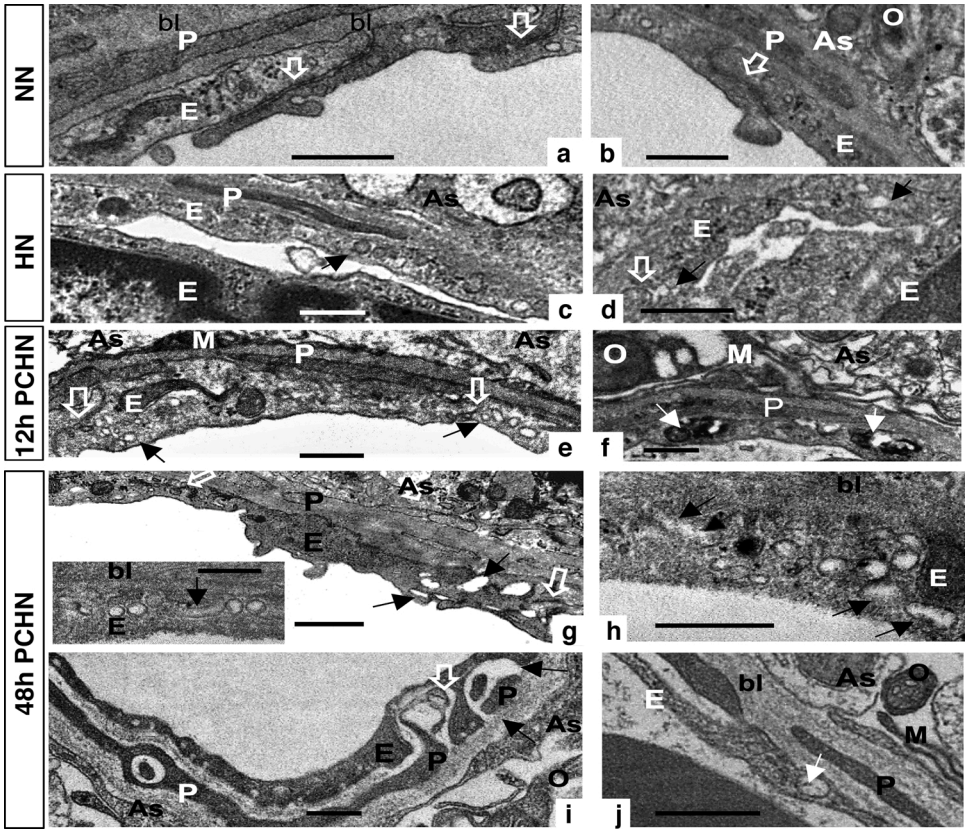

Fig. 2. Pane of fine structure examples of murine thalamus capillary endothelia of NN, HN, 12 h PCHN, 48 h PCHN.
NN a-b: Normal capillary endothelia with junctional complexes, including marginal folds and pericytes surrounded by typical basal laminae.
HN c-d: Collapsed endothelial aspects, where black arrows mark wide round transcytosis vesicles (black arrow in c) and sub-endothelial spaces (black arrow in d).
12 h PCHN e-f: Endothelium and pericyte basal laminae covered by delicate concentrical microglia extensions and oligodendrocyte parts amongst astrocyte end-feet forming sub-endothelial spaces. Junctional complexes appear poorly contrasted entwined with many vesicle profiles (black arrows) and cytoplasm also contains large lysosomal bodies (white plain arrow).
48 h PCHN g–h: Endothelial cells with junctional complexes amid hollow spaces (g) and vesicle profiles forming tubular-like organelles across the endothelial cells; some random tubulo-vesicles appeared to reach the wash out parts of the basal lamina (black arrows in insert of g).
48 h PCHN i-j: Worse damaged capillary aspects. The endothelium appeared thinned, forming abluminal crypts or troughs with altered or lack of basal laminae between endothelial cells and the associated pericytes, creating spaces in continuity with sub-endothelial spaces of the deeply altered brain parenchyma (black arrow in i). Scale bars equal 500 nm. Abbreviations: As: Astrocyte; E: Endothelium; M: Microglia; O: Oligodendrocyte; P: Pericyte; bl: basal laminae; open arrows: junctional complexes; black arrows: endothelium vesicles or tubulo-vesicles and major gaps in basal laminae; white arrows: defects in fine structures.

complexes as well as the marginal fold regions. Random cut, 50−70 nm thick fixed tissue sections, were able to reveal vesicles as elongated parts of a sort of tubulo-vesicular channel system, partly straight or twisted, that reach the abluminal side of the endothelium (Fig. 2 g–h and insert). Within the worst damaged brain lesions, altered or no basal laminae between the endothelial cells and pericytes formed sub-endothelial spaces (Fig. 2 i–j). In order to support the qualitative observations illustrated in Fig. 2, the endothelium alterations were quantified by morphometry (Table 1). Neither endothelium thickness or surface underwent significant variations across experimental groups. On the contrary, the capillary lumen diameter was significantly increased after ODS induction (one-way ANOVA, $p < 0.01$ at 12 h PCHN and $p < 0.05$ at 48 h PCHN compared to NN). By quantifying the density and the size of plasmalemmal vesicles, we confirmed their abnormal size, as enlarged or tubular-shape structures previously visualized at 48 h PCHN (one-way ANOVA, $p < 0.01$ at 48 h PCHN compared to NN). Finally, due to the very local nature of basal laminae abnormalities, it was not possible to find out modifications of its thickness during ODS challenge.

4. Discussion

The seminal hypothesis of BBB opening in ODS arose from autopsy material from the pons containing greenish or yellowish discoloration, subsequent of erythrocyte extravasation and hemoglobin degradation. The mechanistic hypothesis was proposed on the fact that following correction of hyponatremia, a rapid increase of serum osmolality would shift water out of the cells, as a response to correct solute imbalance. Consequently, brain cells lining in front line the blood compartment, as the endothelial and perivascular glial cells, would shrink, which would compromise the stability of intercellular tight junctions and render BBB abnormally permeable to blood-borne factors. Based on the mouse model of ODS, our findings allow now to refine the timing and the degree of BBB breach, and to relate it to oligodendrocyte loss. Using various molecular weight intravascular tracers, we demonstrated that BBB leakage, even to molecules as small as 0.45 kDa, was delayed by 36 h in respect to oligodendrocyte loss. This means that local glial cell defects are independent of blood-derived components, even though the phenomenon's co-localize later in the same demyelinated brain regions [3]. BBB opening was systematically detected at 48 h post-correction, once oligodendrocytes and astrocytes were already lost within ODS lesions. This result suggests that BBB opening is likely a collateral damage, secondary to alterations of astrocyte perivascular feet [28], and in which prominent inflammation might drive the unsealing of inter-endothelial tight junctions. One limitation that should be kept in mind is the possibility that the BBB permeability assays with smallest tracers we performed on whole-brain homogenates, were not sensitive enough to detect, yet relevant, minor and local leakages in specific CNS regions. As recently demonstrated using plasma proteome labeling in mice, many circulatory proteins - smaller than IgG - impregnate the brain parenchyma, beyond the endothelial barrier, in physiological conditions [29].

Unlike the mouse model, ODS rats showed earlier BBB leakages towards small molecules such as horseradish peroxidase (44 kDa) or the split fragment of activated complement C3d (34 kDa), at respectively 3 and 20 h after the correction of hyponatremia [12,13]. Whether this leakage triggers or contributes to local oligodendrocyte damages remains so far unknown. In the mouse model of ODS, BBB opening towards Evans Blue (69 kDa) or IgG (150 kDa) was found starting the second day post-correction of hyponatremia, corroborating the findings of the rat model where a major BBB breakdown is classically described several days after correction. Although BBB is massively disrupted at late timings, remarkably, no extravasation of blood-borne immune cells or erythrocytes were found in other animal models [3,20]. This is a difference with some human post-mortem cases in which the most damaged and demyelinated areas accumulated erythrocytes.

Restricted BBB permeability greatly, but not exclusively, relies on the integrity of inter-endothelial tight junctions. The expression of claudin-1 and occluding was strikingly modified at 48 h post-correction of hyponatremia, yet not earlier. This suggests that inter-endothelial tight junctions might have been transiently or permanently destabilized, which facilitates a paracellular leakage of plasma components into subendothelial spaces. Whether endothelial shrinkage following hypertonic stress or inflammation is responsible for the destabilization of tight junctions will remain an unanswered question. In this model, neuro-inflammation, as evidenced by the progressive accumulation of activated microglia in the lesioned thalamus, was prominent at 48 h post-correction, and thus concomitant with the timing of BBB breakdown. Evidences are numerous to demonstrate that inflammation opens tight junctions and enhances paracellular passage [30,31].

At ultrastructural analysis, even though some changes in the cytoplasm and junctional complexes of the endothelial cells were noticeable 12 h ODS, it is at 48 h post-correction that endothelial linings and associated structures appeared worst impaired. Firstly, the observations that sub-endothelial fluid-filled cavities appeared suggest that tight junction integrity might have been transiently compromised. Those enlargements were seen in or just beneath the basal laminae, and were created in places where astrocyte end-feet or myelin were the most disrupted [20,24,25]. Secondly, ultrastructural morphometry was able to comfort that endothelial intracellular transport and/or transcytosis across the blood-brain barrier was disturbed. We found numerous enlarged tubulo-vesicules that suggested abundant transport across the endothelial cells as channels that reached the abluminal zones into the basal laminae spaces. To remind, ultrastructural findings in the rat model of ODS also evoked higher number of pinocytic vesicles at the level of brain endothelia [6]. It is commonly found that after various forms of injury to the BBB, brain endothelial cells display an increased density of intracellular vesicles [31]. Such vesicles, from round to partly elongated in shape, form tubulo-vesicular structures, and can reflect changes in the intracellular endocytic network. It is often assumed that such an increase in density reflects a higher rate of transcellular passage across the BBB. However, cautious should be taken, since this conclusion

Table 1
Morphometry of thalamus capillaries. Data are shown as mean ± SEM. Following Dunn's multiple comparisons test, the adjusted p-value is expressed in the table as *p < .05, **p < 0.01 for comparison between PCHN and NN; #p < 0.05 for comparison between PCHN and HN. *n*= number of independent capillary images. Abbreviations: NN, normonatremia; HN, hyponatremia; PCHN, post-correction of hyponatremia.

	NN	HN	12 h PCHN	48 h PCHN	Level of significance
Capillary lumen diameter (μm)	3.557 ± 0.387 *n = 18*	3.279 ± 0.317 *n = 7*	6.138 ± 0.718**, # *n = 9*	5.603 ± 0.429*, # *n = 28*	Kruskal–Wallis test, p = 0.0012
Endothelium thickness (μm)	0.341 ± 0.025 *n = 34*	0.342 ± 0.014 *n = 14*	0.286 ± 0.024 *n = 22*	0.287 ± 0.027 *n = 62*	Kruskal–Wallis test, p = 0.1525
Endothelium surface (μm2)	7.691 ± 0.971 *n = 18*	7.385 ± 0.716 *n = 7*	11.46 ± 1.617 *n = 9*	11.13 ± 1.471 *n = 28*	Kruskal–Wallis test, p = 0.2222
Number of vesicles per annulus surface unit (N/μm2)	42.18 ± 3.159 *n = 13*	32.16 ± 4.466 *n = 6*	50.95 ± 2.271 *n = 7*	38.34 ± 4.592 *n = 30*	Kruskal–Wallis test, p = 0.0217
Size of vesicles (nm2)	4389 ± 158 *n = 26*	9201 ± 1767 *n = 12*	6015 ± 1073 *n = 14*	18,230 ± 3780** *n = 58*	Kruskal–Wallis test, p = 0.013
Basal laminae thickness (nm)	112.5 ± 7.965 *n = 24*	98.21 ± 9.785 *n = 14*	84.69 ± 3.88`* *n = 16*	112.5 ± 13.45 *n = 30*	Kruskal–Wallis test, p = 0.0590

is based on morphology alone and not on functional evidences nor on the nature of cargo molecules [32].

Even if we consider an early BBB opening, including leakage of "small" blood-borne molecules potentially toxic, the difficulty resides in explaining the selective loss of oligodendrocytes, next to the relative sparing of neurons within the same demyelinated brain region [22]. Moreover, BBB breakdown is now recognized in many other neurologic disorders, where such a specific pattern of myelin or oligodendrocyte loss does not occur.

In conclusion, we demonstrated that, in the mouse model, BBB permeability – even to small molecules - and endothelium morphology remain unchanged during the first 12 h post-correction of hyponatremia. This timing corresponds to the first clue of oligodendrocyte loss in the future demyelinated brain areas. Altogether, the present results strengthen the idea that BBB disruption is not the primary event during ODS pathology, but account more as a secondary mechanism that might exacerbate later on glial cell or myelin damages.

CRediT authorship contribution statement

Joshua Scalisi: Data curation, Formal analysis, Methodology. **Benoît Balau:** Data curation, Formal analysis, Methodology. **Lynn Deneyer:** Data curation, Formal analysis, Methodology. **Joanna Bouchat:** Data curation, Formal analysis, Methodology. **Jacques Gilloteaux:** Writing - review & editing, Data curation, Formal analysis, Methodology. **Charles Nicaise:** Conceptualization, Writing - original draft.

Declaration of Competing Interest

The authors report no declarations of interest.

Acknowledgments

This research was made possible thanks to the access to the microscope facility of the "Plateforme Technologique Morphologie – Imagerie" (Université de Namur). This research did not receive any specific grant from funding agencies in the public, commercial, or not-for-profit sectors.

Appendix A. Supplementary data

Supplementary material related to this article can be found, in the online version, at doi:https://doi.org/10.1016/j.neulet.2021.135665.

References

[1] B.K. Kleinschmidt-DeMasters, M.D. Norenberg, Rapid correction of hyponatremia causes demyelination: relation to central pontine myelinolysis, Science 211 (1981) 1068–1070.
[2] M.D. Norenberg, K.O. Leslie, A.S. Robertson, Association between rise in serum sodium and central pontine myelinolysis, Ann. Neurol. 11 (1982) 128–135.
[3] F. Gankam Kengne, C. Nicaise, A. Soupart, A. Boom, J. Schiettecatte, R. Pochet, J. P. Brion, G. Decaux, Astrocytes are an early target in osmotic demyelination syndrome, J. Am. Soc. Nephrol. 22 (2011) 1834–1845.
[4] F. Gankam-Kengne, B.S. Couturier, A. Soupart, J.P. Brion, G. Decaux, Osmotic stress-induced defective glial proteostasis contributes to brain demyelination after hyponatremia treatment, J. Am. Soc. Nephrol. 28 (2017) 1802–1813.
[5] B.F. Popescu, R.F. Bunyan, Y. Guo, J.E. Parisi, V.A. Lennon, C.F. Lucchinetti, Evidence of aquaporin involvement in human central pontine myelinolysis, Acta Neuropathol. Commun. 1 (2013) 40.
[6] A.M. Rojiani, E.S. Cho, L. Sharer, J.W. Prineas, Electrolyte-induced demyelination in rats. 2. Ultrastructural evolution, Acta Neuropathol. 88 (1994) 293–299.
[7] H. Takagi, Y. Sugimura, H. Suzuki, S. Iwama, H. Izumida, H. Fujisawa, K. Ogawa, K. Nakashima, H. Ochiai, S. Takeuchi, A. Kiyota, H. Suga, M. Goto, R. Banno, H. Arima, Y. Oiso, Minocycline prevents osmotic demyelination associated with aquaresis, Kidney Int. 86 (2014) 954–964.
[8] A.M. Alleman, Osmotic demyelination syndrome: central pontine myelinolysis and extrapontine myelinolysis, Semin. Ultrasound CT MR 35 (2014) 153–159.
[9] R.H. Sterns, Adverse consequences of overly-rapid correction of hyponatremia, Front. Horm. Res. 52 (2019) 130–142.
[10] S. Adler, J. Martinez, D.S. Williams, J.G. Verbalis, Positive association between blood brain barrier disruption and osmotically-induced demyelination, Mult. Scler. 6 (2000) 24–31.
[11] S. Adler, J.G. Verbalis, D. Williams, Effect of rapid correction of hyponatremia on the blood-brain barrier of rats, Brain Res. 679 (1995) 135–143.
[12] E.A. Baker, Y. Tian, S. Adler, J.G. Verbalis, Blood-brain barrier disruption and complement activation in the brain following rapid correction of chronic hyponatremia, Exp. Neurol. 165 (2000) 221–230.
[13] A.M. Rojiani, J.W. Prineas, E.S. Cho, Electrolyte-induced demyelination in rats. 1. Role of the blood-brain barrier and edema, Acta Neuropathol. 88 (1994) 287–292.
[14] F. Gankam Kengne, A. Soupart, R. Pochet, J.P. Brion, G. Decaux, Re-induction of hyponatremia after rapid overcorrection of hyponatremia reduces mortality in rats, Kidney Int. 76 (2009) 614–621.
[15] Y. Sugimura, T. Murase, S. Takefuji, S. Hayasaka, Y. Takagishi, Y. Oiso, Y. Murata, Protective effect of dexamethasone on osmotic-induced demyelination in rats, Exp. Neurol. 192 (2005) 178–183.
[16] M. Bradl, H. Lassmann, Oligodendrocytes: biology and pathology, Acta Neuropathol. 119 (2010) 37–53.
[17] V.V. Bamm, D.K. Lanthier, E.L. Stephenson, G.S. Smith, G. Harauz, In vitro study of the direct effect of extracellular hemoglobin on myelin components, Biochim. Biophys. Acta 1852 (2015) 92–103.
[18] T.C. Ruijs, A. Olivier, J.P. Antel, Serum cytotoxicity to human and rat oligodendrocytes in culture, Brain Res. 517 (1990) 99–104.
[19] F. Gankam-Kengne, A. Soupart, R. Pochet, J.P. Brion, G. Decaux, Minocycline protects against neurologic complications of rapid correction of hyponatremia, J. Am. Soc. Nephrol. 21 (2010) 2099–2108.
[20] J. Bouchat, B. Couturier, C. Marneffe, F. Gankam-Kengne, B. Balau, K. De Swert, J. P. Brion, L. Poncelet, J. Gilloteaux, C. Nicaise, Regional oligodendrocytopathy and astrocytopathy precede myelin loss and blood-brain barrier disruption in a murine model of osmotic demyelination syndrome, Glia 66 (2018) 606–622.
[21] J. Bouchat, J. Gilloteaux, V. Suain, D. Van Vlaender, J.P. Brion, C. Nicaise, Ultrastructural analysis of thalamus damages in a mouse model of osmotic-induced demyelination, Neurotox. Res. 36 (2019) 144–162.
[22] J. Gilloteaux, J. Bouchat, J.P. Brion, C. Nicaise, The osmotic demyelination syndrome: the thalamic neurons resilience is verified with electron microscopy, Ultrastruct. Pathol. 44 (2020).
[23] C. Nicaise, D. Mitrecic, P. Demetter, R. De Decker, M. Authelet, A. Boom, R. Pochet, Impaired blood-brain and blood-spinal cord barriers in mutant SOD1-linked ALS rat, Brain Res. 1301 (2009) 152–162.
[24] M.S. Soyfoo, A. Konno, N. Bolaky, J.S. Oak, D. Fruman, C. Nicaise, M. Takiguchi, C. Delporte, Link between inflammation and aquaporin-5 distribution in submandibular gland in Sjogren's syndrome? Oral Dis 18 (2012) 568–574.
[25] S. Nag, Ultracytochemical studies of the compromised blood-brain barrier, Methods Mol. Med. 89 (2003) 145–160.
[26] M. Simionescu, N. Simionescu, G.E. Palade, Morphometric data on the endothelium of blood capillaries, J. Cell Biol. 60 (1974) 128–152.
[27] G. Clough, Relationship between microvascular permeability and ultrastructure, Prog. Biophys. Mol. Biol. 55 (1991) 47–69.
[28] C. Nicaise, C. Marneffe, J. Bouchat, J. Gilloteaux, Osmotic demyelination: from an oligodendrocyte to an astrocyte perspective, Int. J. Mol. Sci. 20 (2019).
[29] A.C. Yang, M.Y. Stevens, M.B. Chen, D.P. Lee, D. Stähli, D. Gate, K. Contrepois, W. Chen, T. Iram, L. Zhang, R.T. Vest, A. Chaney, B. Lehallier, N. Olsson, H. du Bois, R. Hsieh, H.C. Cropper, D. Berdnik, L. Li, E.Y. Wang, G.M. Traber, C. R. Bertozzi, J. Luo, M.P. Snyder, J.E. Elias, S.R. Quake, M.L. James, T. Wyss-Coray, Physiological blood-brain transport is impaired with age by a shift in transcytosis, Nature 583 (2020) 425–430.
[30] N.J. Abbott, Inflammatory mediators and modulation of blood-brain barrier permeability, Cell. Mol. Neurobiol. 20 (2000) 131–147.
[31] A.S. Lossinsky, R.R. Shivers, Structural pathways for macromolecular and cellular transport across the blood-brain barrier during inflammatory conditions, Rev. Histol. Histopathol. 19 (2004) 535–564.
[32] R. Villaseñor, J. Lampe, M. Schwaninger, L. Collin, Intracellular transport and regulation of transcytosis across the blood-brain barrier, Cell. Mol. Life Sci.: CMLS 76 (2019) 1081–1092.